Journal of ELECTRONIC MATERIALS, Vol. 38, No. 6, 2009
DOI: 10.1007/s11664-009-0769-4
© 2009 TMS
Regular Issue Paper

Tensile and Fatigue Behaviors of Aged Cu/Sn-4Ag Solder Joints

Q.K. ZHANG,[1] H.F. ZOU,[1] and Z.F. ZHANG[1,2]

1.—Shenyang National Laboratory for Materials Science, Institute of Metal Research, Chinese Academy of Sciences, Shenyang 110016, P.R. China. 2.—e-mail: zhfzhang@imr.ac.cn

Tensile properties and stress-controlled fatigue fracture behaviors of Cu/Sn-4Ag solder joints aged at 180°C for different times were systematically investigated. It was found that the tensile strength of the solder joints decreased with increasing aging time and that the fracture mode changed from ductile to brittle. The fatigue life of the solder joints also decreased with increasing aging time. For most of the solder joints, fatigue cracks tended to initiate around the Cu/Cu_6Sn_5 interfaces due to the strain incompatibility and local strain concentration on a micro-scale, and they then propagated within the solder proximately along the Cu/Cu_6Sn_5 interfaces. The samples aged for different times or tested under different stress amplitudes had similar fractography morphologies, which consisted mainly of a propagation region, covered by solder, and a final fracture region. Based on the experimental observations above, the corresponding interfacial fatigue failure mechanisms were discussed in terms of different influencing factors.

Key words: Lead-free solders, interface, intermetallic compounds (IMCs), fatigue crack, fractography

INTRODUCTION

Although traditional Sn-37Pb eutectic solder alloys have been used widely in microelectronics assembly, many industrialized countries have legislated to limit their usage, because lead and Pb-based compounds have been cited by the Environmental Protection Agency (EPA) as one of the top 17 chemical poisons that are the greatest threat to human life and the environment.[1] Now, developing viable alternative lead-free solders has become significantly important in the microelectronics industry, because soldering not only provides electronic connections, but also ensures the mechanical reliability of solder joints under the service conditions. Therefore, it has been recognized that one of the major concerns for the integrity of the solder interconnection is the damage mechanisms at the solder/substance interfaces under various practical service conditions. Furthermore, solders are increasingly expected to perform in some dynamic service environments where stress and strain distributions change with time. In particular, the advance in high-density electronic packaging technology has set higher standards for the mechanical reliability of the interconnections. Not only are the uniaxial tensile or shear properties important, but also the fatigue properties of Pb-free solder joints have great significance.[2,3]

The Sn-Ag series solder alloy is one of the most promising Pb-free solder candidates, because it has a relatively low melting point, good soldering ability, and excellent mechanical properties. In recent years there have been many investigations concerning the tensile and fatigue properties of Sn-Ag solder or solder joints.[4–13] However, most of these studies have been based only on the experiments performed to evaluate the reliability of the solder joints. Although the solder/substance interface is crucial for the mechanical integrity of the solder joints, few studies so far have focused on the microscopic interfacial damage behaviors. In particular, there have been very limited studies on the fatigue behavior of solder/substance interfaces, which is more valuable in practice.[14,15] Therefore, in order to obtain some reliable fatigue data about solder/substance interfaces and to have a better

(Received April 6, 2008; accepted March 11, 2009; published online April 10, 2009)

understanding of the mechanisms of interfacial fatigue damage, we systematically investigated the behaviors of tensile and stress-controlled fatigue fractures of Cu/Sn-4Ag solder joints aged at 180°C. Furthermore, it is expected that this research may provide a new approach for reliability evaluation of the Cu/solder interfaces.

EXPERIMENTAL PROCEDURE

In this study the Cu single crystal plate was grown from oxygen-free high conductivity (OFHC) Cu of 99.999% purity by the Bridgman method in a horizontal furnace. The solder alloy was Sn-4Ag, which we prepared by melting high purity (>99.99%) tin and silver at 800°C for 30 min in vacuum. According to the Sn-Ag binary diagram, the equilibrium microstructure of the Sn-4Ag alloy is composed of proeutectic plate-like Ag_3Sn coarse grains and a eutectic microstructure of Sn and needle-like Ag_3Sn particles.[10]

The Cu single crystal plate was first spark-cut into small blocks, and the surfaces for soldering were carefully polished with a diamond polishing agent. After they had been air dried, a soldering paste was spread on the polished area; a Sn-4Ag alloy sheet was placed on the paste to ensure sufficient wetting reaction. Graphite plates were clamped on the sides of the Cu samples with the solder paste, to avoid the outflow of the molten solder. The prepared samples were bonded in an oven at a temperature of 260°C for 10 min to evaporate the rosin flux and then cooled down in air. Some of the soldered samples were isothermally aged for 4 days and 16 days at a temperature of 180°C.[14,15] After that, both the as-reflowed and aged samples were spark-cut into tensile and fatigue specimens, and the side surfaces were firstly ground with 2000# SiC abrasive paper and then carefully polished with 1 μm diamond powder for the microstructural observations of the solder/Cu interface. The dimensions of tensile and fatigue specimens are presented in Fig. 1.

Both tensile and fatigue tests were carried out with an Instron 8871 fatigue testing machine at room temperature in air. Tensile tests were performed under a cross-beam speed of 0.005 mm s^{-1} to obtain a strain rate of approximately 1.25×10^{-4} s^{-1}. All the fatigue tests were stress-controlled and performed under a symmetrical sinusoid wave with a frequency of 2 Hz. A stress ratio (R), defined as the ratio of the stress amplitude (σ_a) to the tensile strength of the samples (σ_b), was employed to illustrate the relative stress intensity. The stress ratio was chosen in the range of 0.50–0.95, varied for the samples aged for different times. Microstructures and fracture surfaces of the specimens were observed in a LEO scanning electronic microscope, which revealed the initiation and propagation of the fatigue crack and the final fracture morphologies.

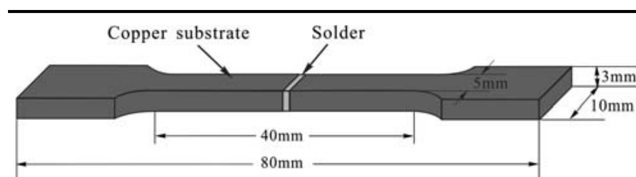

Fig. 1. Illustration of tensile and fatigue specimens.

RESULTS AND DISCUSSION

Morphology and Growth Kinetics of Interfacial Intermetallic Compounds

During the initial soldering process, the intermetallic compound (IMC) layer displayed a scallop-like morphology forming along the interface of the Sn-4Ag/Cu joints, as shown in Fig. 2a. Analysis by energy dispersive x-ray (EDX) spectroscopy indicated that the IMC layer was the Cu_6Sn_5 phase, with an average thickness of approximately 2 μm. Figure 2d shows the morphology of the Cu_6Sn_5 grains in the as-soldered sample. It can be seen that the Cu_6Sn_5 grains are spherical. After isothermal aging at 180°C for 4 days, the IMC/solder interface became quite flat, and the IMC thickness increased to about 6 μm, as shown in Fig. 2b. Meanwhile, the scallop-like Cu_6Sn_5 layer changed to a planar type with duplex layers of Cu_6Sn_5/Cu_3Sn, and the spherical Cu_6Sn_5 grains became typical equiaxed ones (see Fig. 2e). The flattening process requires that the growth of the IMC should be faster in the valleys of the scallop than in the peaks.[16] After isothermal aging for 16 days, the total IMC thickness had increased to approximately 11 μm, and there was no obvious coarsening of the IMC/solder interface, as shown in Fig. 2c. The morphology of the Cu_6Sn_5 grains was similar to that of the samples aged for 4 days, but the grains became larger, as seen in Fig. 2e and f. The growth of the interfacial IMC layers during the aging process was considered to be controlled by a diffusion mechanism, and the growth rate of the Sn-4Ag/Cu interface was approximate to the SnAgCu/polycrystalline Cu and the SnAgCu/Cu single crystal interfaces.[17–20] In addition, if we compare Fig. 2b with Fig. 2a, we find that there is a little coarsening of the needle-like Ag_3Sn grains in the solder, which may induce a slight decrease of the yield strength of the solder.

Tensile Property and Fracture Behavior

Figure 3 shows the tensile stress–displacement curves of the solder joints aged for different times. It indicates that the tensile strength (σ_b) of the solder joints had dropped from 59.2 MPa (as-soldered samples) to 46.8 MPa (samples aged for 4 days) and 38.0 MPa (samples aged for 16 days). This tendency is in agreement with many previous results.[21,22] In addition, the yield strengths of those samples are in the range of 15–20 MPa, and the samples exhibited strong strain hardening during the tensile test, as

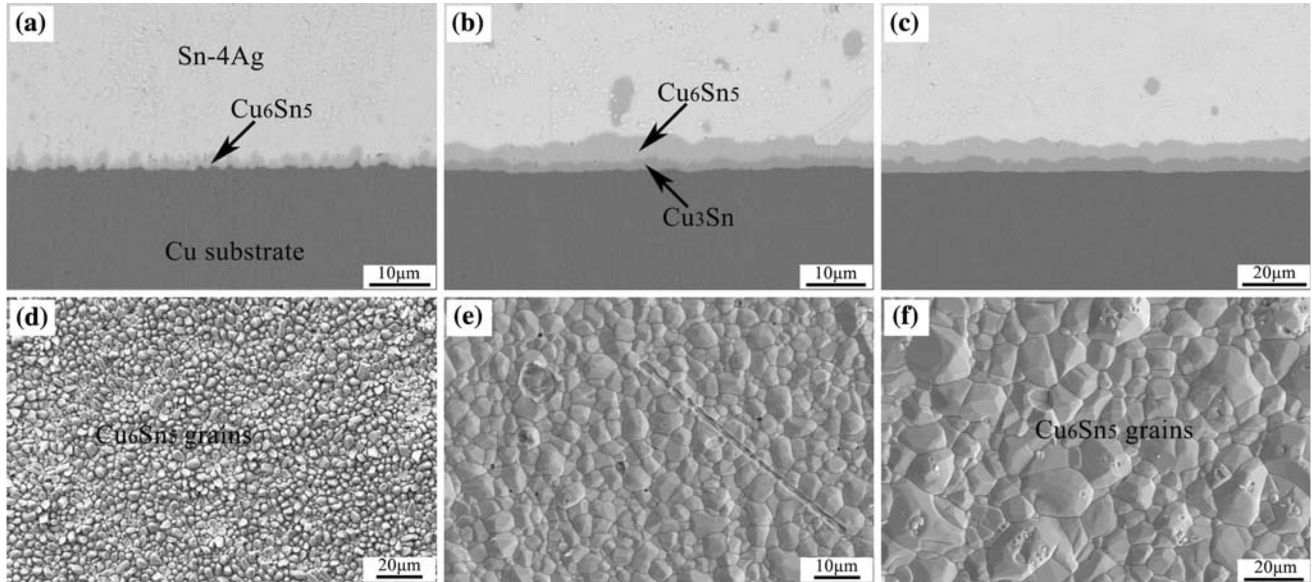

Fig. 2. Morphology and evolution of interfacial IMCs after aging at 180°C for different times. (a) Interfacial morphology of as-soldered sample; (b) sample aged for 4 days; (c) sample aged for 16 days; (d) grain morphology of as-soldered sample; (e) sample aged for 4 days and (f) 16 days.

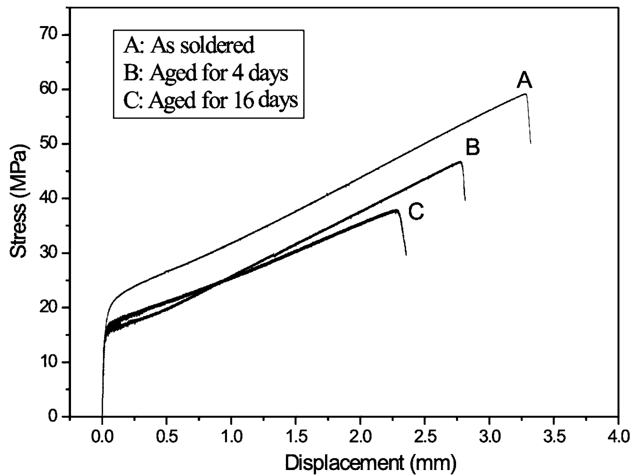

Fig. 3. Stress–displacement curves of solder joints aged at 180°C for different times.

shown in Fig. 3. Since the solder layer is only a small fraction of the whole sample, a tensile stress–displacement curve of the whole sample should be quite similar to that of the Cu single crystal; thus, the yield and strong strain-hardening behavior should mainly result from the plastic deformation of the Cu single crystal. Although the stress amplitudes are always higher than the yield strength of the Cu single crystal during a fatigue test (≥20 MPa), the Cu substrate should not display much plasticity, due to the strong work hardening.

Figure 4 shows the tensile fractographic morphologies of the samples aged for different times, from which one can conjecture the microscopic tensile fracture mechanisms for the samples processed for different aging times. The as-soldered sample exhibited a typical ductile rupture feature, as indicated by the numerous dimples shown in Fig. 4a. There are some cracked IMCs at the bottom of the dimples (Fig. 4b), indicating that the micro-scale cracks firstly initiated at the top of the IMC layer and then propagated into the solder, along a special angle, to form a dimple. In contrast, the samples aged for 16 days displayed the typical feature of trans-granular brittle rupture in the interior of the Cu_6Sn_5 grains (Fig. 4d). The fracture mechanism of the samples aged for 4 days is more complicated. According to their fractographies, shown in Fig. 4c, it seems that the samples broke in a mixed mode or that a ductile-to-brittle transition occurred because both ductile dimples and brittle IMCs coexisted on the fracture surface. As a result, it can be predicted that the fracture mode may be transformed from ductile to brittle when the interfacial IMC thickness increases to approximately 6 μm; the transition is quite consistent with the decrease in the tensile strength.[5]

As the Young's modulus, yield strength and hardness of Cu_6Sn_5 and Cu_3Sn phases are much higher than those of the solder alloy and Cu substrate, the external stress cannot be the only reason for the fracture of the interfacial IMCs during tensile testing. In fact, due to the decrease in the volume during continuous growth of Cu_6Sn_5 and Cu_3Sn layers, residual transformation stress accumulates at the interface of solder/Cu.[23–25] Additionally, the simulation of stress distribution indicates that there is a severe stress concentration at the corner of the Cu/Cu_6Sn_5 interface, which is induced by the strain incompatibility.[5] Therefore, for the aged samples, the interfacial IMCs are easily broken at a low stress and exhibit a brittle fracture feature.

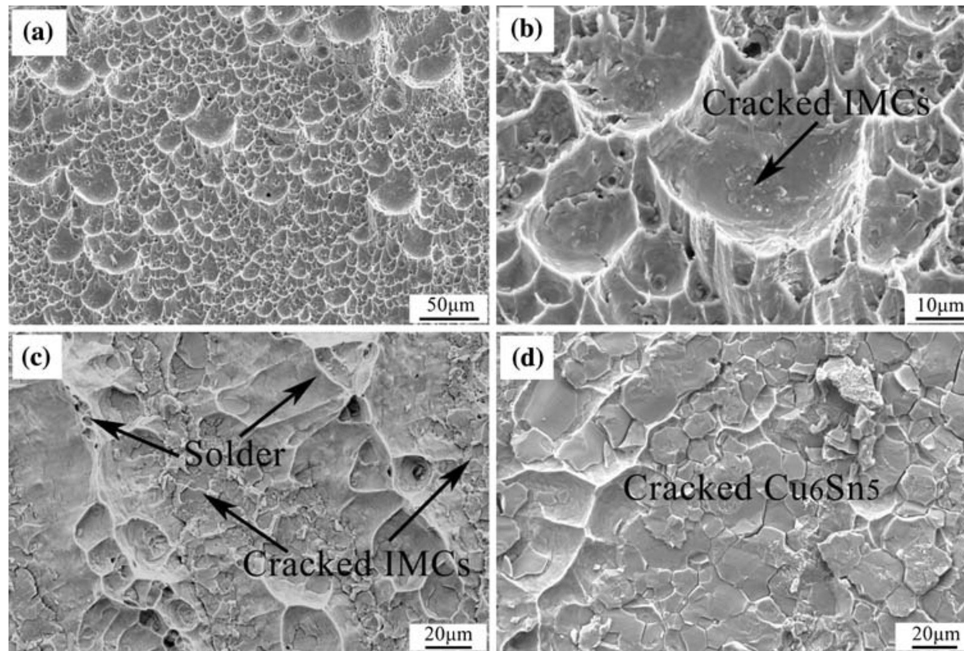

Fig. 4. Tensile fractography morphologies showing (a) ductile fracture of the as-soldered sample; (b) magnified dimples of the ductile fracture surface; (c) fracture of the samples aged for 4 days and (d) 16 days.

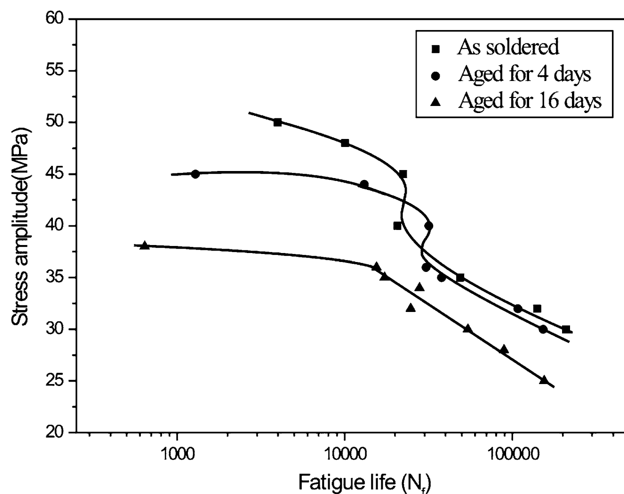

Fig. 5. S–N curves of joint samples aged at 180°C for different times.

Fatigue Behavior

The stress amplitude (σ_a)–fatigue life (N_f) relationship (S–N curve) of specimens aged for different times is shown in Fig. 5. When the stress amplitude is low (e.g., $\sigma_a \leq 35$ MPa), the fatigue life displays an approximately exponential increase with decreasing stress amplitude. Additionally, it is obvious that the fatigue life of the as-soldered samples is close to that of the samples aged for 4 days, but is obviously longer than that of the samples aged for 16 days. This indicates that a short aging time (e.g., 4 days) might slightly affect the fatigue life of the joint samples, but that a long aging time (e.g., 16 days) may markedly worsen the fatigue properties of the joint samples. The fatigue failure processes and the effect of adhesive strength on fatigue life will be discussed later in detail.

When the stress amplitude is higher (e.g., $\sigma_a \geq 40$ MPa), it is obvious that the fatigue life abnormally deviates from the conventional range of low-cycle fatigue life. When the stress amplitude is between 40 MPa and 45 MPa, the S–N curve has a nearly upright ascent, and then it descends with increasing stress amplitude, which is similar to that of a Pb-rich solder alloy.[26] The abnormal range of as-reflowed samples is a little bit higher than that of the samples aged for 4 days. The increase in abnormal fatigue life under higher stress amplitude may be caused by a yield of the solder, because the yield strength of Sn-4Ag solder is approximately 40–50 MPa under the current strain rate.[3,27] When the stress amplitude is higher than the yield strength of the solder, the solder will first yield to release the strain incompatibility between the solder and the interfacial IMC. It has been reported that aging often induces a small drop in the yield strength, due to the coarsening of the needle-like Ag_3Sn particles in the solder alloy.[8,28] Therefore, the S–N curve of samples aged for 4 days deviates in the lower stress amplitude range in comparison with that of the as-soldered ones. For the samples aged for 16 days, there is no such abnormal phenomenon, because the stress amplitude is lower than the yield strength of the solder. For the samples aged for 4 days and 16 days, the stress ratio can be very high, with relatively long and steady fatigue lives. Thus, it seems that, at the same stress ratio, fatigue lives of the aged samples are longer.

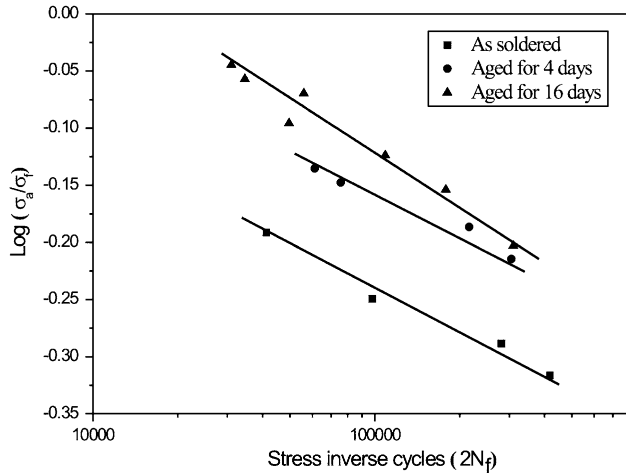

Fig. 6. Dependence of log (σ_a/σ_f) on reversal number ($2N_f$) of the joined samples aged at 180°C for different times ($\sigma_a < \sigma_y$).

However, when the stress amplitude increases to a value close to the tensile strength, the fatigue life of the sample will decrease rapidly to less than 1000, which may correspond to an obvious transition of the fatigue fracture mechanisms.

It is common to use the Basquin equation to describe the relationship between the applied stress amplitude and the fatigue life. For the solder joints tested at a low stress amplitude, the equation is:

$$\Delta\sigma/2 = \sigma_a = \sigma'_f (2N_f)^b \quad (1)$$

where σ_a is the stress amplitude and σ'_f is the fatigue strength coefficient, which is close to the fracture strength of the samples (σ_f). Since the solder between the two pieces of Cu is very thin, its plastic deformation is restrained by the Cu substrate, so that necking of the solder can be neglected. Here, we hold an approximation that $\sigma_f = 1.05\sigma_b$, as the strain of the sample is 5% on average. N_f is the fatigue life and b is the fatigue strength exponent. The stress amplitude exhibits an approximately linear relationship with the stress inverse cycles on a log–log plot, as shown in Fig. 6. The fatigue strength exponent can be calculated from the slope of the fit lines, and the values of the as-soldered samples and samples aged for 4 days and 16 days are $b_0 = -0.124$, $b_4 = -0.113$ and $b_{16} = -0.146$, respectively. Beyond that, one can make a prediction of the approximate fatigue lives of the solder joints when their fracture strengths and the applied stress amplitudes are given.

Fatigue Fracture Process

To investigate the initiation and propagation mechanisms of fatigue cracks, we chose some samples at fixed cycles for side surface observations. The results showed that the samples aged for different times had similar crack initiation mechanisms. In Fig. 7, an as-soldered sample tested at a stress amplitude of 35 MPa was employed to reveal the initiation mechanism. Figure 7a shows the side surface morphology of the as-soldered sample after 5000 cycles. Close to the interfacial IMC, severe plastic deformation of the solder was observed, due to the stress concentration at the solder/IMC interface. In fact, such stress concentration has been proven by simulation of the stress distribution at the Cu/solder interface.[5] In light of the great difference of mechanical properties between the solder and the IMC, especially the hardness, it is easy to understand the severe strain incompatibility and

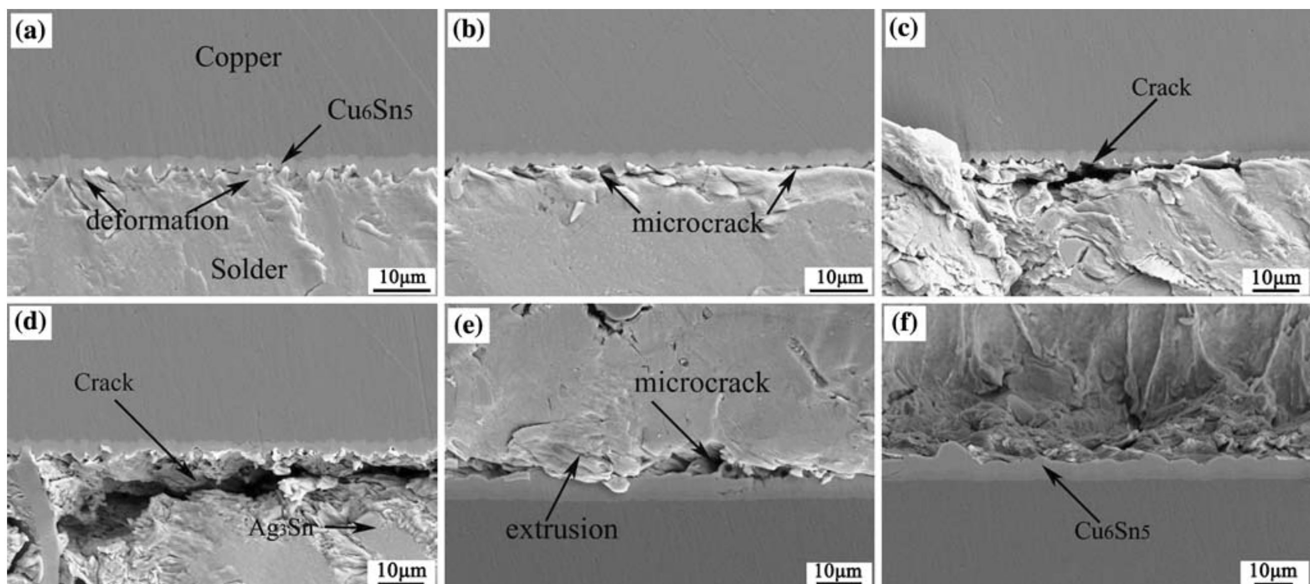

Fig. 7. Side surface showing (a) deformation of solder; (b) micro-cracks; (c) initiation and (d) propagation of fatigue cracks; (e) extrusion and micro-crack near the Cu_6Sn_5/solder interface of the aged sample; (f) side surface of the fractured sample.

stress concentration that exists near the interfaces.[23,24] After 10,000 cycles, some superficial micro-cracks appeared at the solder/Cu_6Sn_5 interface, as shown in Fig. 7b. With increasing number of cycles, plastic deformation at the solder/IMC interface became more and more severe. The micro-cracks linked up with each other to form a long initial crack and propagated into the solder near the solder/Cu_6Sn_5 interface, as shown in Fig. 7c. With further increasing number of cycles, fatigue cracks remained in the solder and kept propagating (Fig. 7d). According to Fig. 7e, in which the sample had been aged for 4 days and tested at a stress amplitude of 35 MPa for 10,000 cycles, it can be predicated that the original micro-crack initiation mechanism of the aged samples will be a little bit different from that of the as-soldered samples. Besides, although the plastic deformation of the solder close to the interfacial IMC was severe, the initial fatigue cracks of the Cu/Sn-4Ag solder joints appeared just at the solder/Cu_6Sn_5 interface, rather than in the deformed solder. The perfect residual interfacial IMC on the fracture surface shown in Fig. 7f provided clear evidence. In addition, some reports have indicated that the plate-like Ag_3Sn grains can be regarded as a strengthening phase to improve the resistance to fatigue cracking.[11] In our study, inhomogeneous plastic deformation with a core of plate-like Ag_3Sn grains in the solder adjacent to the interface was observed, as shown in Fig. 7d, which may have decreased the fatigue life of the solder joints by promoting the crack initiation. However, as there are only a few plate-like Ag_3Sn grains at the interface where cracks are easily initiated, the plate-like Ag_3Sn compound may actually have little effect on fatigue crack initiation.

The propagation path and fracture mechanism of fatigue cracks can be predicated from the fractographic morphologies of solder joints. Observations showed that the samples aged for different times and tested at different stress amplitudes had similar fatigue fracture surfaces. Figure 8 shows the typical fractographic morphologies of the fatigued samples. The macroscopic image of the fatigue fracture surface is illustrated in Fig. 8a. It is obvious that there are two regions in general: (1) a region of fatigue crack propagation, covered by deformed solder and (2) a final fracture region with a flat morphology on a macroscale. As the fatigue cracks were often initiated at the sample edge, the fracture surface in this region was quite smooth, due to the effects of friction and crack closure, as shown in Fig. 8b. In contrast, the region of fatigue crack propagation was quite rough and covered by a layer of deformed solder, as shown in Fig. 8c. Combined with the former side-surface observations in Fig. 7, it is obvious that fatigue cracks were propagated in the solders close to the solder/Cu_6Sn_5 interface. Little IMC was found in the former two regions. Another difference from the conventional surface of the fatigue fracture of engineering materials is that there is no fatigue striation observed in the region of fatigue crack propagation, as in Fig. 8c.

The morphology of the final fracture region is a bit complex. Though all the samples finally failed in a brittle mode, there were always two types of fracture modes observed in the same sample, i.e., inter-granular fracture (see Fig. 8d) and trans-granular fracture (see Fig. 8f). Figure 8e shows the interface of the inter-granular fracture and trans-granular fracture. For the inter-granular fracture, cracking

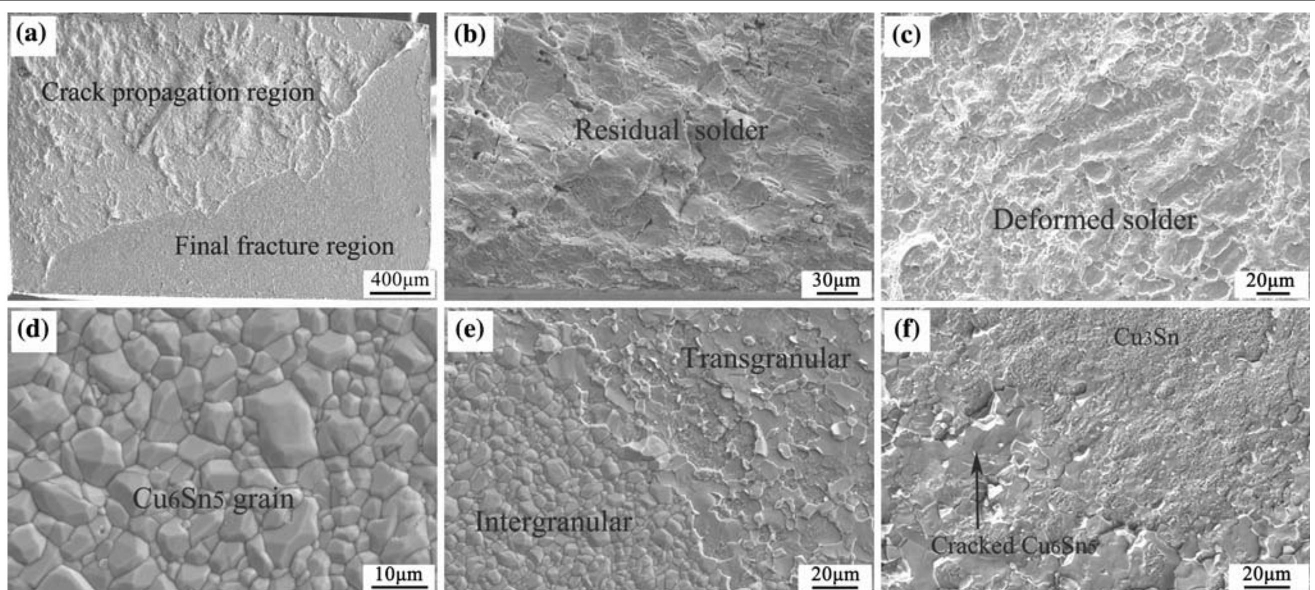

Fig. 8. Fatigue fracture surface. (a) Macroscopic image; (b) fractography morphologies, showing fatigue crack origin; (c) region of fatigue crack propagation, with deformed solder; (d) inter-granular fatigue fracture along the Cu_6Sn_5/solder interface; (e) transition region from inter-granular to trans-granular fatigue fracture; (f) trans-granular fracture along the Cu_6Sn_5/Cu_3Sn interface.

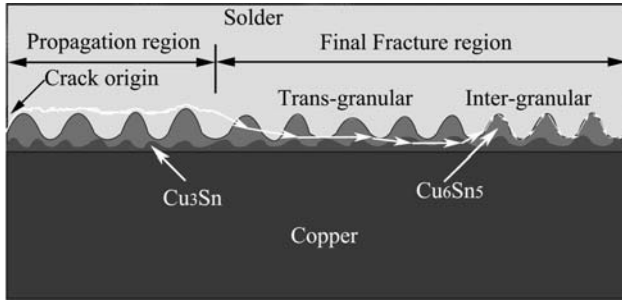

Fig. 9. Illustration of fatigue crack propagation and final fracture mode.

often occurred at the interface of the Cu_6Sn_5 grains and the solder; and the interfacial Cu_6Sn_5 grains remained intact after the final fracture. In contrast, for the trans-granular fracture mode, cracking occurred in the interior of IMCs. For the samples aged for 16 days or subjected to higher stress amplitudes, even some Cu_3Sn grains could be found at the final fracture surface (see Fig. 8f).

It can be concluded from the foregoing observations and discussion that specimens aged for different times have similar processes for the initiation and propagation of fatigue cracks when the stress amplitude is relatively low. Figure 9 illustrates the whole process of fatigue failure. Firstly, the solder close to the Cu_6Sn_5/solder interface deforms severely due to the stress concentration under the cyclic loading; micro-cracks appear at the interface, caused by the strain incompatibility between the two phases. With increasing number of cycles, the micro-cracks link up and are propagated into the solder adjacent to the solder/Cu_6Sn_5 interface. The effective loading area is reduced, and the real stress applied to the solder joints increases with the propagation of fatigue cracks. When the real stress approaches the tensile strength, final brittle fracture will occur in an inter-granular or trans-granular mode, as shown in Fig. 9.

Fatigue Life Determinant

The analysis above demonstrates that the IMCs do not break during the initiation and propagation of fatigue cracks, and the thickness of the IMC layer seems to have little effect on the strain incompatibility. So, it is reasonable to assume that the interfacial microstructure (or IMC thickness) has no significant influence on the mechanism of fatigue crack initiation and the following propagation behavior. Beyond that, if the effect of aging on the yield strength of the solder is neglected, samples aged for different times but at the same stress amplitude can be considered to have the same crack initiation process. The fatigue life (N_f) is considered to consist of a crack initiation cycle (N_i) and propagation cycle (N_p). For specimens aged for different times, the crack initiation cycles should be approximately equal when they were deformed under the

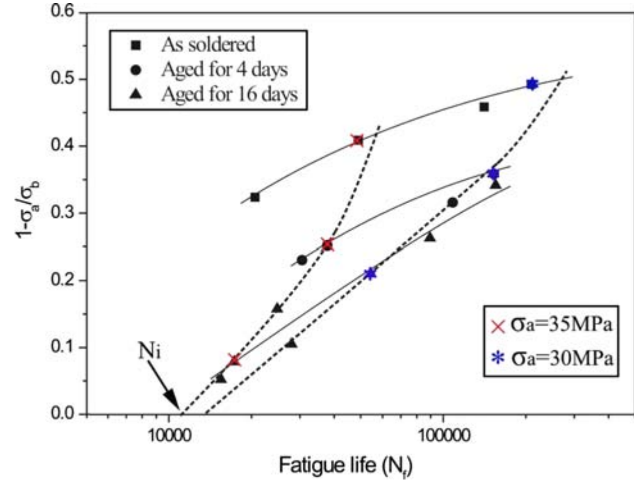

Fig. 10. Fatigue life determinant analysis of the solder joints aged for different times at the same stress amplitude.

same stress amplitude and their crack propagation rates are also similar. Therefore, only the difference in the fracture strength determines the different propagation cycles and thus different fatigue lives.

Figure 10 qualitatively illustrates the relationship between the fatigue life and the stress ratio of specimens aged for different times but at the same stress amplitude. To avoid the effect of yield of the solder, we have illustrated only the specimens tested at the stress amplitudes of 30 MPa and 35 MPa. In this scheme, the y-axis ($1 - \sigma_a/\sigma_b$) represents the proportion of the crack propagation region (see Fig. 9) and the x-axis corresponds to the exponential-expressed cyclic number, considering that the fatigue crack propagation rate has an approximately exponential relationship with the real stress applied to the samples. According to the foregoing discussion, specimens tested at the same stress amplitude have the same number of crack initiation cycles (N_i), which corresponds to the intercepts of the broken lines in the scheme. However, if we consider that the crack propagation cycle (N_p) is proportional to the proportion of the crack propagation region in Fig. 10, the deviation of the as-soldered samples is a little serious; the fatigue lives of the as-soldered samples are shorter than expected. In fact, the strength of the solder is affected by the thermal treatment history, and the yield strength of the solders in as-soldered specimens is higher. As fatigue cracks propagate in solder, the strength of the solder in specimens is crucial to crack propagation rates and fatigue lives. Therefore, the relatively higher strength corresponds to a lower fracture toughness, so the rate of fatigue crack propagation is higher in the as-soldered samples, resulting in a lower N_p. Although N_i of as-soldered specimens may be higher, its proportion in fatigue life is much lower than that of N_p; thus, the fatigue lives of as-soldered specimens are shorter than expected.

CONCLUSIONS

Tensile and fatigue fracture behaviors of Sn-4Ag/Cu solder joints aged at 180°C for different times were investigated. Based on the experimental results and analysis, the following conclusions can be drawn.

The tensile strength (σ_b) of Sn-4Ag/Cu solder joints decreases with increasing aging time or interfacial IMC thickness; the tensile fracture mechanism also changes from ductile to a ductile–brittle mixed mechanism and, finally, to a trans-granular brittle mode. The deterioration of interfacial strength and the change of fracture modes have a close relationship with the accumulation of residual transformation stress during growth of the interfacial IMCs.

The fatigue life exhibits an approximately exponential increase with the decrease of stress amplitude when the stress amplitude is much lower. With increasing stress amplitude, the S–N curve may firstly present a nearly upright ascent and then drop rapidly. Solder joints aged for different times exhibit similar processes of fatigue damage. During cyclic loading, micro-cracks are initiated at the interface of the solder/IMC, due to strain incompatibility, then they link up to form long fatigue cracks and are propagated into the solder adjacent to the solder/Cu_6Sn_5 interface. When the real stress amplitude approaches the fracture strength, final brittle fracture will occur.

The thickness of the interfacial IMC has little influence on the initiation mechanism and propagation paths of the fatigue crack; the fatigue lives are affected though dominating the fracture strength. Joint samples aged for different times and subjected to fatigue at the same stress amplitude have the same crack initiation mechanism and similar crack initiation cycles; only the difference of the tensile strength leads to different crack propagation cycles and fatigue lives.

ACKNOWLEDGEMENTS

The authors would like to acknowledge F. Yang, Q.Q. Duan, Q.S. Zhu, P. Zhang, G, Yao, W. Gao and H.H. Su for sample preparation, tensile and fatigue tests and scanning electron microscopy observations. This work was financially supported by the National Basic Research Program of China, under Grant No. 2004CB619306, the National Outstanding Young Scientist Foundation, under Grant No. 50625103, and the "Hundred of Talents Project" by Chinese Academy of Sciences.

REFERENCES

1. E.P. Wood and K.L. Nimmo, *J. Electron. Mater.* 23, 709 (1994). doi:10.1007/BF02651363.
2. H.K. Kim and K.N. Tu, *Appl. Phys. Lett.* 67, 2002 (1995). doi:10.1063/1.114767.
3. M. Abtew and G. Selvaduray, *Mater. Sci. Eng. R* 27, 95 (2000).
4. S. Kikuchi, M. Nishimura, K. Suetsugu, and T. Ikari, *Mater. Sci. Eng. A* 319–321, 475 (2001). doi:10.1016/S0921-5093(01)01031-0.
5. H.T. Lee, M.H. Chen, H.M. Jao, and T.L. Liao, *Mater. Sci. Eng. A* 358, 134 (2003). doi:10.1016/S0921-5093(03)00277-6.
6. O. Fouassier, J.M. Heintz, J. Chazelas, P.M. Geffory, and J.F. Silvain, *J. Appl. Phys.* 100, 043519 (2004). doi:10.1063/1.2244478.
7. J.J. Sundelin, S.T. Nurmi, T.K. Lepisto, and E.O. Ristolainen, *Mater. Sci. Eng. A* 420, 55 (2006).
8. Y. Ding, C.Q. Wang, Y.H. Tian, and M.Y. Li, *J. Alloys Compd.* 428, 274 (2007). doi:10.1016/j.jallcom.2006.02.069.
9. C. Kanchanomai, Y. Miyashita, Y. Mutoh, and S.L. Mannan, *Mater. Sci. Eng. A* 345, 90 (2003). doi:10.1016/S0921-5093(02)00461-6.
10. H.D. Solomon, *J. Electron. Packag.* 113, 102 (1991). doi:10.1115/1.2905374.
11. J. Zhao, Y. Miyashita, and Y. Mutoh, *Int. J. Fatigue* 23, 723 (2001). doi:10.1016/S0142-1123(01)00034-2.
12. A. Boulaajaj, J.M. Cabrera, and J.M. Prado, *Eng. Fail. Anal.* 15, 220 (2008). doi:10.1016/j.engfailanal.2007.06.001.
13. C. Lea, *A Scientific Guide to Surface Mount Technology* (GB-Port Erin, British Isles: Electrochemical Publications Ltd., 1988).
14. Q.S. Zhu, Z.F. Zhang, Z.G. Wang, and J.K. Shang, *J. Mater. Res.* 23, 78 (2008). doi:10.1557/jmr.2008.0015.
15. Q.S. Zhu, Z.F. Zhang, J.K. Shang, and Z.G. Wang, *Mater. Sci. Eng. A* 435–436, 588 (2006). doi:10.1016/j.msea.2006.07.100.
16. T.Y. Lee, W.J. Choi, and K.N. Tu, *J. Mater. Res.* 17, 291 (2002). doi:10.1557/JMR.2002.0042.
17. A. Zribi, A. Clark, L. Zavalij, D. Borgesem, and E.J. Cotts, *J. Electron. Mater.* 30, 1157 (2001). doi:10.1007/s11664-001-0144-6.
18. X. Deng, G. Piotrowski, J.J. Williams, and N. Chawla, *J. Electron. Mater.* 32, 1403 (2003). doi:10.1007/s11664-003-0108-0.
19. W. Yang, R.W. Messier, and L.E. Felton, *J. Electron. Mater.* 23, 765 (1994). doi:10.1007/BF02651371.
20. X. Ma, F.J. Wang, Y.Y. Qian, and F. Yoshida, *Mater. Lett.* 57, 3361 (2003). doi:10.1016/S0167-577X(03)00075-2.
21. N.R. Bonda and I.C. Noyan, *IEEE Trans. Compon. Packag. Manuf. Technol. A* 19, 208 (1990). doi:10.1109/95.506106.
22. S.P. Yu, M.H. Hon, and M.C. Wang, *J. Electron. Mater.* 29, 237 (2000). doi:10.1007/s11664-000-0149-6.
23. M. Dao, N. Chollacoop, K.J. Van Vliet, T.A. Venkatesh, and S. Suresh, *Acta Mater.* 49, 3899 (2001). doi:10.1016/S1359-6454(01)00295-6.
24. X. Deng, N. Chawla, K.K. Chawla, and M. Koopman, *Acta Mater.* 52, 4291 (2004). doi:10.1016/j.actamat.2004.05.046.
25. Z. Mei, A.J. Sunwoo, and J.W. Morris Jr., *Metall. Trans. A* 23, 857 (1992).
26. S. Vaynman, M.E. Fine, and D.A. Jeannotte, *Metall. Trans. A* 19, 1051 (1988).
27. J. Glazer, *Int. Mater. Rev.* 40, 2 (1995).
28. P. Suna, C. Andersson, X.C. Wei, Z.N. Cheng, D.K. Shangguan, and J.H. Liu, *J. Alloys Compd.* 437, 169 (2007). doi:10.1016/j.jallcom.2006.07.121.